Vol 18 No 1, January 2009
1674-1056/2009/18(01)/0251-08

Chinese Physics B

Dislocation formation and twinning from the crack tip in Ni_3Al: molecular dynamics simulations*

Xie Hong-Xian(谢红献)[a)†], Wang Chong-Yu(王崇愚)[a)b)c)],
Yu Tao(于 涛)[a)], and Du Jun-Ping(杜俊平)[a)]

[a)] *Central Iron and Steel Research Institute, Beijing* 100081, *China*
[b)] *International Centre for Materials Physics, Chinese Academy of Sciences, Shenyang* 110016, *China*
[c)] *Department of Physics, Tsinghua University, Beijing* 100084, *China*

(Received 29 June 2008; revised manuscript received 20 August 2008)

The mechanism of low-temperature deformation in a fracture process of $L1_2$ Ni_3Al is studied by molecular dynamic simulations. Owing to the unstable stacking energy, the $[0\bar{1}1]$ superdislocation is dissociated into partial dislocations separated by a stacking fault. The simulation results show that when the crack speed is larger than a critical speed, the Shockley partial dislocations will break forth from both the crack tip and the vicinity of the crack tip; subsequently the super intrinsic stacking faults are formed in adjacent {111} planes, meanwhile the super extrinsic stacking faults and twinning also occur. Our simulation results suggest that at low temperatures the ductile fracture in $L1_2$ Ni_3Al is accompanied by twinning, which is produced by super-intrinsic stacking faults formed in adjacent {111} planes.

Keywords: molecular dynamic, crack, Shockley partial dislocation，stacking fault
PACC: 6185, 4630N, 6170G, 6170N

1. Introduction

It is well known that nickel-based superalloy is one of the most important structural materials for advanced aircraft turbine blades. The mechanical properties of Ni_3Al and its derivatives have been a subject of extensive experimental study and theoretical modelling for the past three decades. The strength anomaly was investigated by several groups experimentally[1] and numerically.[2−5] Using computer simulation techniques, Yamaguchi *et al*[6] and Paidar *et al*[7] studied the structure of the dislocation core in Ni_3Al and indicated that superdislocation would be dissociated into partial dislocations separated by stacking fault. Baluc and Schaublin[8] studied the deformation substructures of Ni_3Al by means of weak-beam transmission electron microscopy (TEM) observations and gave the dislocation modes of superdislocations by combining weak-beam TEM observations with weak-beam TEM image simulations.

Generation of deformation twins associated with the formation of superlattice stacking faults has been reported by a number of research workers under various creep loading conditions at elevated temperatures.[9−13] Creep deformation substructures in superalloy were investigated after small-strain creep at intermediate temperatures using the conventional TEM and the high-resolution TEM.[11] It was established that at intermediate temperatures microtwinning caused by the passage of Shockley partial dislocations in successive {111} planes was the dominant deformation process at low applied stresses. Microtwinning during intermediate temperature creep of polycrystalline Ni-based superalloys was studied by using the same method above, and the conclusion was that microtwinning occurred via the sequential motions of identical 1/6[11-2] Shockley partials in successive (111) planes.[12] The role of ⟨112⟩ {111} slip in the asymmetric nature of creep of single crystal superalloy CMSX-4 was also studied at temperatures of 1223 and 1023 K,[13] and the TEM analysis indicated that twinning nucleation was dependent upon the activation of appropriate ⟨110⟩ {111} type slip within the matrix channels. Superlattice stacking fault formation and twinning during creep in nickel-based superalloy were reported experimentally by Knowles and Chen,[14] and it was found that the formation of high temperature twinning could always be associated with

*Project supported by the National Basic Research Program of China (Grant No 2006CB605102) and the National Natural Science Foundation of China (Grant No 90306016).
†Corresponding author. E-mail: hongxianxie@163.com

the super extrinsic stacking fault (SESF). Crack propagation in single crystal Ni_3Al at room temperature was also studied experimentally,[15,16] and the results showed that the room temperature failures were highly localized, often knife-edge sharp and nearly parallel to the primary slip plane. However, at low temperatures, the effects of superdislocation formation and twinning in Ni_3Al on its fracture toughness have not been explained clearly. It is known that the possibility of local deformation has a notable influence on the crack growth and toughness of the material. Therefore, the investigation of the deformation mechanism on the crack tip in Ni_3Al is of great importance for the study of the mechanical behaviours of intermetallic alloys. This paper is aimed at providing an insight into the formation of dislocation and deformation twins from low temperature fractures in single crystal Ni_3Al and how they are correlated with the formation of superlattice stacking faults.

In the present work, the molecular dynamics (MD) method (which is a powerful tool to study the nature of materials[17−19]) is used to study the dislocation formation and twinning from the crack tip in Ni_3Al. The interatomic interaction is expressed by Voter–Chen-type embedded atom method (EAM) potential,[20] which is very successful in the study on the Ni–Al system.[21−25] The rest of the present paper is organized as follows. We present an uncracked model and the detailed results on the energy analyses in Section 2. Section 3 is devoted to the study on the structure evolution of dislocations breaking forth from the crack tip. Finally, the simulation results and main conclusions drawn from the present study are summarized in Section 4.

2. Perfect sample

In order to study the formation of dislocation at the crack tip, we first consider an uncracked structure. Figure 1 is the projection of the Ni_3Al lattice onto a (111) plane. The sample is oriented along the axes $x = [\bar{1}\bar{1}2]$, $y = [111]$, and $z = [1\bar{1}0]$. The simulation domain comprises 240 atomic planes in the x direction, 60 planes in the y direction, and 120 planes in the z direction. Periodic boundary conditions are applied in the x and z directions, while free boundary conditions are imposed in the y direction. The sample is divided into two parts by the (111) plane; the lower part is fixed and the upper part is gradually displaceable (step by step) in the (111) plane along the following routes (see Fig.1): route I ($a \to b \to c \to d$); route II ($a \to e \to g$); route III ($a \to b \to e \to f \to g$). During this rigid sliding in the (111) plane, the fault energy of the system can be calculated as

$$E_{\mathrm{POT}}(R,0) = (E_{\mathrm{POT}}(R) - E_{\mathrm{POT}}(0))/A_{111}, \qquad (1)$$

where R is the relative shear displacement between the lower fixed part and the upper displaceable part; A_{111} is the total area of the (111) plane; $E_{\mathrm{POT}}(R)$ and $E_{\mathrm{POT}}(0)$ are the energies of the sample at the relative shear displacements R and 0, respectively.

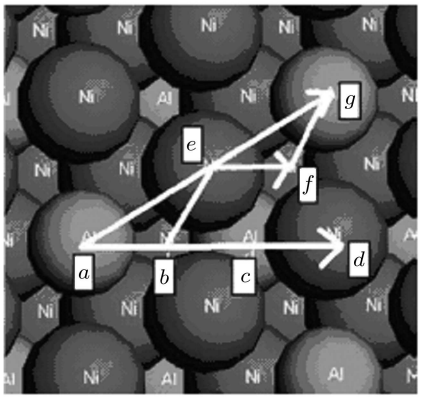

Fig.1. The Ni_3Al lattice is projected onto a (111) plane.

Figure 2 shows the variation in fault energy with the dimensionless shear displacement during rigid sliding of the sample, and the calculated results are summarized in Table 1. From Fig.2(a), we can see that there are two peaks located at $0.5b_1$ and $2.0b_1$, separately, where b_1 is the magnitude of the Burgers vector of the 1/6[112] Shockley partial dislocation. The fault energy located at $0.5b_1$ is the unstable stacking energy γ_{usa1}, according to Rice's work,[25] which represents the energy barrier required for the generation of a $1/6[\bar{1}\bar{1}2]$ Shockley partial dislocation. It is also found that the fault energy located at $2.0b_1$ is $3.440\,\mathrm{J/m^2}$. Furthermore, we can calculate the unstable stacking energy $\gamma_{\mathrm{usc}} = E_{\mathrm{POT}}(2.0b_1, 0) - E_{\mathrm{POT}}(1.0b_1, 0) = 3.440\,\mathrm{J/m^2} - 0.142\mathrm{J/m^2} = 3.298\,\mathrm{J/m^2}$, which represents the energy barrier that has to be overcome from the point b to the point d (see Fig.1). The fault energy at $1.0b_1$ is the complex stacking fault (CSF) energy produced by the motion of a $1/6[\bar{1}\bar{1}2]$ Shockley partial dislocation in the (111) plane.

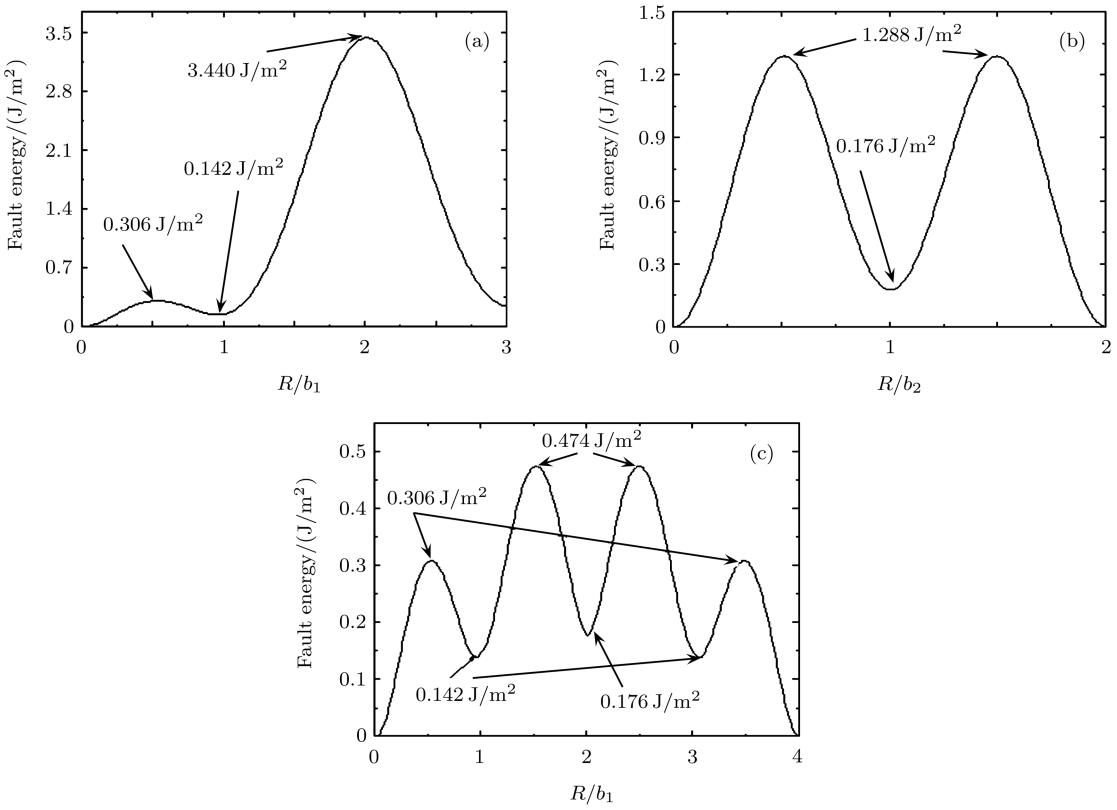

Fig.2. Variations in fault energy with dimensionless shear displacement during rigid sliding of the sample along route I (a), route II (b), and route III (c) separately, where R is the relative shear displacement between the lower fixed part and the upper displaceable part; $b_1 = \sqrt{6}a_0/6$ and $b_2 = \sqrt{2}a_0/2$ are the Burgers vectors of the 1/6[112] Shockley partial dislocation and the 1/2[110] partial dislocation, respectively; a_0 is the lattice constant of Ni_3Al.

Table 1. Comparison between the calculated energies (J/m^2) and the energies measured and cited from other work, where $E_{\rm APB}$ and$E_{\rm CSF}$ are the APB energy and the CSF energy, respectively.

	this work	EAM	experiment	*Ab initio*
$E_{\rm CSF}$ (111)	0.142	0.202[26]	0.206[27]	0.223[28]
$E_{\rm APB}$ (111)	0.176	0.142[20] 0.252[26]	0.180 ± 0.030[29] 0.180[27]; 0.175[31]	0.188[30] 0.172[28]
$\gamma_{\rm usa1}$	0.306			
$\gamma_{\rm usa2}$	0.332			
$\gamma_{\rm usa3}$	0.298			
$\gamma_{\rm usa4}$	0.164			
$\gamma_{\rm usb}$	1.288			
$\gamma_{\rm usc}$	3.298			

Figure 2(b) represents the variation in fault energy in route II. The peak located at $0.5b_2$ is the unstable stacking energy $\gamma_{\rm usb}$, which represents the energy barrier required for the generation of a 1/2[101] dislocation. The fault energy at $1.0b_2$ is the antiphase boundary (APB) energy produced by the motion of a 1/2[101] dislocation in the (111) plane. Figure 2(c) displays the variation in fault energy in route III. The fault energies at $1.0b_1$ and $3.0b_1$ are the CSF energies in the (111) plane and the fault energy at $2.0b_1$ is the APB energy in the (111) plane. There are four kinds of unstable stacking energies:

$$\begin{aligned}
\gamma_{\rm usa1} &= 0.306\,{\rm J/m^2},\\
\gamma_{\rm usa2} &= E_{\rm POT}(1.5b_1, 0) - E_{\rm POT}(1.0b_1, 0)\\
&= 0.474\,{\rm J/m^2} - 0.142\,{\rm J/m^2} = 0.332\,{\rm J/m^2},\\
\gamma_{\rm usa3} &= E_{\rm POT}(2.5b_1, 0) - E_{\rm POT}(2.0b_1, 0)\\
&= 0.474\,{\rm J/m^2} - 0.176\,{\rm J/m^2} = 0.298\,{\rm J/m^2},
\end{aligned}$$

and

$$\gamma_{\rm usa4} = E_{\rm POT}(3.5\ b_1, 0) - E_{\rm POT}(3.0\ b_1, 0) = 0.306\,{\rm J/m^2} - 0.142\,{\rm J/m^2} = 0.164\,{\rm J/m^2}.$$

From Table 1, it can be seen that $E_{\rm APB}$ calculated in the present work is in good agreement with the experimental values and the theoretical results obtained from other authors, $E_{\rm CSF}$ in the present work is slightly smaller than those in Refs.[26–28]. However, the discrepancy between the CSF energies does not affect the dissociation of the superdislocation, because the unstable stacking energies in route III are much smaller than those in routes I and II. From the energy viewpoint, the $[0\bar{1}1]$ superdislocation can be dissociated into Shockley partial dislocations separated by stacking fault.[8] To test the above analysis, a cracked sample is simulated in Section 3.

3. Cracked sample

In this part, we consider a pre-existing atomically sharp crack embedded in the computational cell with relaxed atomic displacement. The whole system is initially displaced by the anisotropic elastic solution[32] for the critical stress intensity factor. As shown in Fig.3, the sample is oriented at $x = [10\bar{1}]$, $y = [010]$, and $z = [101]$. The crack surface is (010) plane, and the crack front is oriented along the [101] direction. To simulate the experiment of uniaxial tensile deformation, we use the homogeneous dynamic loading[33,34] in MD simulation. The crack is loaded in mode I, i.e. the top and bottom layers of atoms in the $y = [010]$ direction are loaded by external forces. Periodic boundary conditions are imposed along the crack front to simulate plane strain conditions, while free boundary conditions are applied in the x axis (the direction of crack propagation). This geometry makes slip planes of the $\{111\}$ type available for activation. The simulated system comprises 300 atomic layers along the $[10\bar{1}]$ direction, 200 atomic layers along the [010] direction, and 12 atomic layers along the [101] direction, thus a total of 180000 atoms are included. We have tested the system with a larger number of planes in the x and y directions ($x = 400, y = 300$) and found that the maximum value of the crack speed and the configuration evolution on the crack tip are insensitive to the system size. The initial crack length is $l_0 = 9\,{\rm nm}$. Newton's equations of motion in MD are solved by the Gear algorithm.[35] The time integration step Δt is 5×10^{-15}s, i.e. $\Delta t = 5 \times 10^{-15}$s. We perform the simulations under the condition of constant stress (12.5 GPa) and constant temperature (5 K). The temperature of the system keeps invariant in the loading process, which is obtained by scaling the instantaneous speeds of all atoms with an appropriate Maxwell–Boltzmann distribution at a specified temperature.

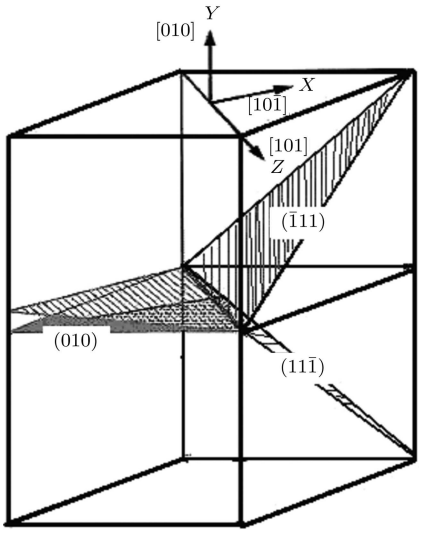

Fig.3. Schematic illustration of the $\{010\}\langle 101\rangle$ crack in Ni_3Al.

In the MD simulation, a brittle fracture without any crack tip plasticity is observed in the initial 10 ps. The variation in crack speed with time is plotted in Fig.4, from which it is found that in the initial 4 ps the crack recedes slightly because the external stress has not reached the crack tip, then it increases rapidly and reaches a maximum value of 990 m/s at 10 ps, and then it drops more rapidly. After 14 ps the propagation of the crack ceases, simultaneously the crack tip

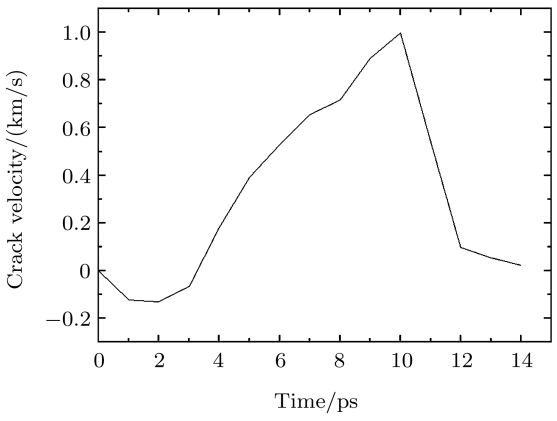

Fig.4. Variation in crack speed with time.

region is disordered, and then dislocations break forth from the crack tip (see Fig.5). We have calculated the Rayleigh wave speed (C_R) of Ni_3Al and compared it with the crack speed, and we find that the maximum value of the crack speed is $0.39C_R$. Our simulation result is in good agreement with measurements on brittle amorphous materials,[36−38] which indicates an instability-driven picture of dynamic fracture occurring above a critical speed ($0.4C_R$).

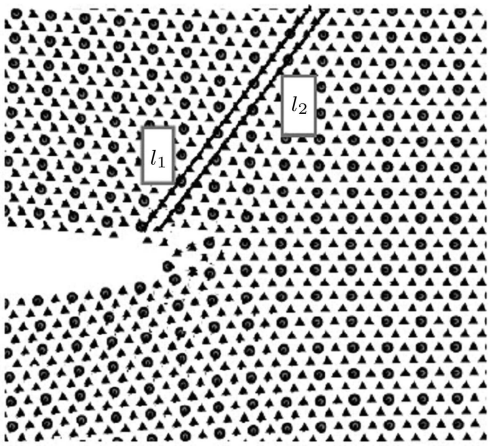

Fig.5. Atomic configuration near the crack tip at 14 ps (projected onto the (101) plane), where solid circles and triangles denote Al atoms and Ni atoms, respectively.

Because both the $(11\bar{1})$ plane and the $(\bar{1}11)$ plane are symmetric, we only need to show the upper part (containing the $(\bar{1}11)$ plane) of the crack. In the MD simulation, it is observed that at 14 ps the Shockley partial dislocations break forth along the line l_1 that is shown in Fig.5, in a $(\bar{1}11)$ slip plane. Figure 6 shows the atomic configuration near the crack tip along the line l_1 at 14 ps, and the Shockley partial dislocation that has arrived at the line A. On the right of line A the crystal is perfect. Between the lines A and D, there exist three Shockley partial dislocations, which combine forming a $1/3[12\bar{1}]$ dislocation according to the following equation:

$$1/6[\bar{1}1\bar{2}] + 1/6[12\bar{1}] + 1/6[211] = 1/3[12\bar{1}]. \quad (2)$$

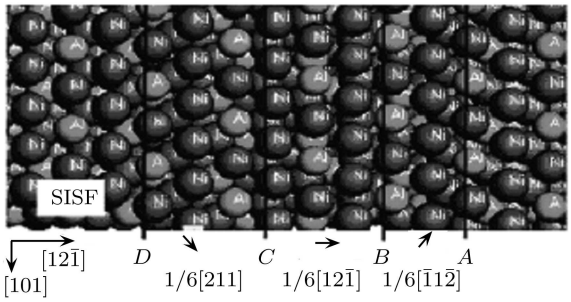

Fig.6. Atomic configuration near the crack tip along the line l_1 at 14 ps (projected onto the $(\bar{1}11)$ plane).

On the left of the line D, there appears a superlattice intrinsic stacking fault (SISF), which is produced by the glide of the $1/3[12\bar{1}]$ dislocation. Then the $1/6[\bar{1}1\bar{2}]$ and $1/6[12\bar{1}]$ Shockley partial dislocations move forward, and combine forming the $1/2[01\bar{1}]$ dislocation according to the following reaction (see Fig.7):

$$1/6[\bar{1}1\bar{2}] + 1/6[12\bar{1}] = 1/2[01\bar{1}]. \quad (3)$$

While the $1/6[211]$ Shockley partial dislocation remains there, the dislocation $1/3[12\bar{1}]$ is dissociated into $1/2[01\bar{1}]$ and $1/6[211]$ partial dislocations separated by the antiphase boundary (APB). The reaction equation can be written as follows:

$$1/3[12\bar{1}] = 1/2[01\bar{1}] + \mathrm{APB} + 1/6[211]. \quad (4)$$

The $1/6[211]$ Shockley partial dislocation and the $1/6[12\bar{1}]$ Shockley partial dislocation that has newly broken forth from the crack tip along the line l_1 at 16 ps, constitute the dislocation $1/2[110]$ (see Fig.7). The reaction equation can be written as follows:

$$1/6[211] + 1/6[12\bar{1}] = 1/2[110]. \quad (5)$$

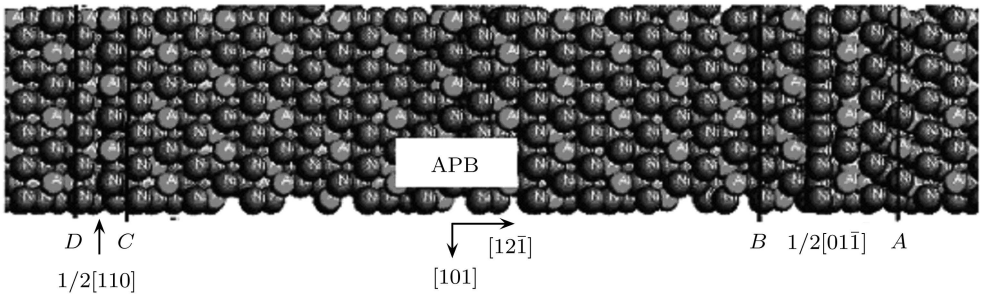

Fig.7. Atomic configuration near the crack tip along the line l_1 at 17 ps (projected onto the $(\bar{1}11)$ plane).

At 15 ps, a 1/6[211] Shockley partial dislocation breaks forth from the vicinity of the crack tip and propagates along the line l_2 that is marked in Fig.5, and at 17 ps, another 1/6[12$\bar{1}$] Shockley partial dislocation also breaks forth from the same point and propagates along the same line. The atomic configuration near the crack tip along the line l_2 at 17 ps is plotted in Fig.8. From Fig.8 we can see the following points: both on the right of the line A and on the left of the line F, the crystal is perfect; the 1/6[211] and 1/6[12$\bar{1}$] Shockley partial dislocations are separated by the CSF; the APB is produced by the motion of the two Shockley partial dislocations; there is a hole between the line E and the line F, which is created by the partial dislocations breaking forth from this region. In order to show the global configuration of the crack tip, we display the atomic configuration on the crack tip projected onto the (101) plane in Fig.9.

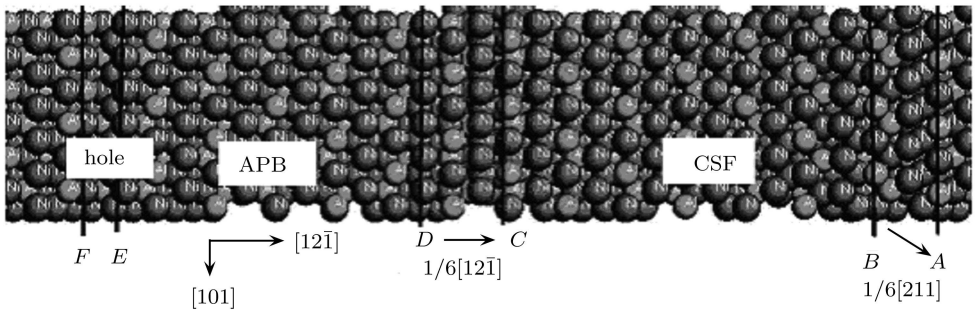

Fig.8. Atomic configuration near the crack tip along the line l_2 at 17 ps (projected onto the ($\bar{1}$11) plane).

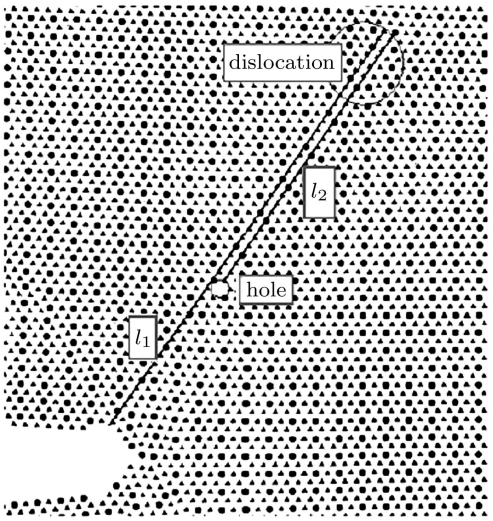

Fig.9. Atomic configuration near the crack tip at 17 ps (projected onto the (101) plane), where solid circles and triangles denote Al atoms and Ni atoms, respectively.

From 18 to 22 ps, dislocations break forth from the (11$\bar{1}$) plane rather than from the ($\bar{1}$11) plane. Figure 10 shows the atomic configuration near the crack tip along the line l_1 at 23 ps, and the 1/2[110] dislocation formed at 17 ps that is dissociated according to the following reaction:

$$1/2[110] = 1/6[211] + \mathrm{SISF} + 1/6[12\bar{1}]. \qquad (6)$$

The 1/6[211] Shockley partial dislocation propagates forward and arrives at the line A, however the 1/6[12$\bar{1}$] Shockley partial dislocation remains there. Subsequently the SISF between the two Shockley partial dislocations is formed. Furthermore, from Fig.10 we can see that a new Shockley partial dislocation 1/6[$\bar{1}$1$\bar{2}$] breaks forth near the crack tip, and it combines the partial dislocation 1/6[12$\bar{1}$], thereby constitutes the dislocation 1/2[01$\bar{1}$] according to the following reaction:

$$1/6[12\bar{1}] + 1/6[\bar{1}1\bar{2}] = 1/2[01\bar{1}]. \qquad (7)$$

The dislocation 1/2[01$\bar{1}$] is located at the line C.

Figure 11 plots the atomic configuration near the crack tip along the line l_2 at 23 ps. At 23 ps, a 1/6[$\bar{1}$1$\bar{2}$] Shockley partial dislocation breaks forth from the hole between the lines C and D and reaches line A, subsequently leaving the SISF behind.

As is well known, in the $L1_2$ perfect lattice, the stacking sequence of the {111} planes is $\ldots ABCABCABC\ldots$. This makes stacking faults or multilayer twins be able to occur in the {111} planes, and it can be illustrated by looking at Fig.12. Suppose that the left planes $ABCABC$ in Fig.12 are the planes in a perfect $L1_2$ crystal, and that the next plane on the right of the C is an A plane. If the A plane and all planes on the right of it are displaced by the vector $1/3\langle 112\rangle$, the A plane moves into a B plane, and the

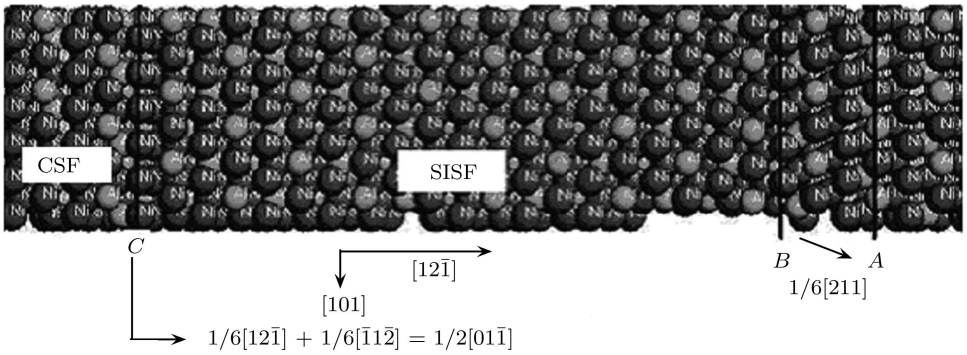

Fig.10. Atomic configuration near the crack tip along the line l_1 at 23 ps (projected onto the ($\bar{1}$11) plane).

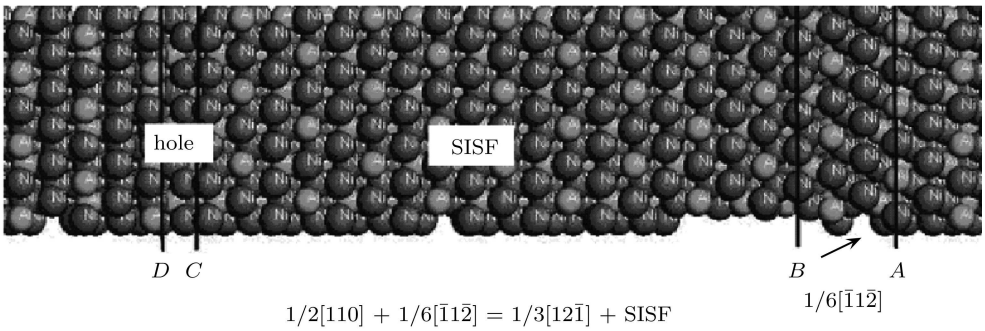

Fig.11. Atomic configuration near the crack tip along the line l_2 at 23 ps (projected onto the ($\bar{1}$11) plane).

planes on the right of it undergo the transitions: $A \to B$, $B \to C$ and $C \to A$, and the resulting fault is an SISF. Then the shear along the same direction with a further displacement of the next right planes will experience the following transitions: $C \to A$, $A \to B$ and $B \to C$. This shear displacement is marked by the arrows in Fig.12, from which it is clearly seen that the passage of SISF generating dislocation in two adjacent planes results in the same change in lattice as that caused by an SESF, which leads to a twinning in the $L1_2$ lattice. From Figs.9 and 10 we can see that the SISF along the lines l_1 and l_2 is formed and accompanied with a partial dislocation on the edge of the stacking fault. Figure 13 shows the detailed stacking sequence of ($\bar{1}$11) planes in a tip region after the breaking forth of the partial dislocation. It can be seen that the stacking sequence changes from $\ldots ABCAB\ldots$ to $\ldots ABCBA\ldots$. This is SESF and stacking fault twinning. According to the present work and Chen's work,[14] we can conclude that the formation of twinning can always be associated with the SESF at low and high temperatures.

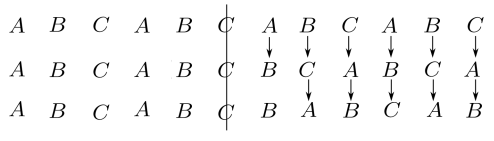

Fig.12. The stacking fault sequence in an $L1_2$ structure, resulting in twinning formation.

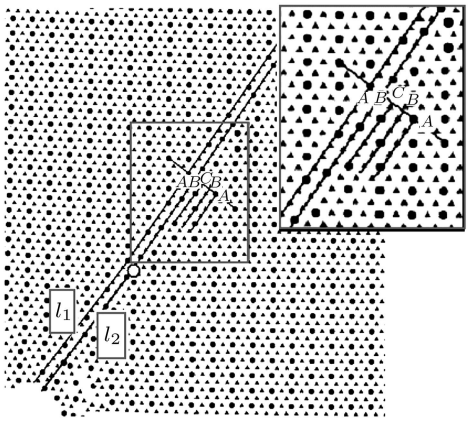

Fig.13. Atomic configuration near the crack tip at 23 ps (projected onto the (101) plane), where solid circles and triangles denote Al atoms and Ni atoms, respectively.

4. Summary

In the present work, we use the MD method to explore the process of the dislocation formation and twinning from mode I crack tip in Ni_3Al. The unstable stacking energy, APB energy, and CSF energy are calculated, and the calculated results are in agreement with the experiment values and the theoretical results obtained from other authors. From the energy viewpoint, the $[0\bar{1}1]$ superdislocation will be dissociated into Shockley partial dislocations separated by stacking faults. The simulation results show that at low temperatures when the crack speed is larger than $0.39C_R$, the Shockley partial dislocations break forth from both the crack tip and the vicinity of the crack tip; subsequently the SISFs are formed in adjacent {111} planes and the SESF and twinning can be seen. As is well known, dislocation and twinning are two major defects determining the mechanical properties of materials. The present work has analysed the dislocation configuration and twinning formation in Ni_3Al in detail, and it will be helpful for understanding the mechanical properties of Ni_3Al.

References

[1] Korner A 1991 *Philos. Mag.* A **63** 407

[2] Chou C T and Hirsch P B 1993 *Philos. Mag.* A **68** 1097

[3] Benoit Devincre, Patrick Veyssière, Ladislas P Kubin and Georges Saada 1997 *Philos. Mag.* A **75** 1263

[4] Ngan A H W, Wen M and Woo C H 2004 *Comput. Mater. Sci.* **29** 259

[5] Choi Y S, Dimiduk D M, Uchic M D and Parthasarathy T A 2007 *Philos. Mag.* **87** 1939

[6] Yamaguchi M, Paidar V, Pope D P and Vitek V 1982 *Philos. Mag.* A **45** 867

[7] Paidar V, Yamaguchi M, Pope D P and Vitek V 1982 *Philos. Mag.* A **45** 883

[8] Baluc N and Schaublin R 1996 *Philos. Mag.* A **74** 113

[9] Ardakani A, McLean M and Shollock B A 1999 *Acta Mater.* **47** 2593

[10] Kakehi K 1999 *Scripta Mater.* **41** 461

[11] Viswanathan G B, Peter M Sarosi, Deborah H Whitis and Michael J Mills 2005 *Mater. Sci. Eng.* A **400–401** 489

[12] Viswanathan G B, Karthikeyan S, Saros P M, Unocic R R and Mills M J 2006 *Philos. Mag.* **86** 4823

[13] Knowles D M and Gunturi S 2002 *Mater. Sci. Eng.* A **328** 223

[14] Knowles D M and Chen Q Z 2003 *Mater. Sci. Eng.* A **340** 88

[15] Ming Dao, Bimal K Kad and Robert J Asaro 1997 *Philos. Mag.* A **75** 443

[16] Shan Z W, Wu X, Liu L, Yang J H and Xu Y B 2001 *Mater. Sci. Technol.* **17** 1398

[17] Zhang J M, Huang Y H, Xu Ke-Wei and Ji Vincent 2007 *Chin. Phys.* **16** 210

[18] Chen J, Chen D Q and Zhang J L 2007 *Chin. Phys.* **16** 2779

[19] Chen L Q, Wang C Y and Yu T 2008 *Chin. Phys.* B **17** 662

[20] Voter A F and Chen S P in: Siegel R W, Weertman J R and Sinclair R (eds) 1987 *MRS Symposia Proceedings* **82** p175

[21] Rey C, Garcí-Rodeja J and Gallego L J 1996 *Phys. Rev.* B **54** 2942

[22] Farkas D, Roqueta D, Vilette A and Ternes K 1996 *Modell. Simul. Mater. Sci. Eng.* **4** 359

[23] Zhu T and Wang C Y 2005 *Phys. Rev.* B **72** 014111

[24] Xie H X, Wang C Y and Yu T 2008 *J. Mater. Res.* **23** 1597

[25] Rice J R and Bettz G E 1994 *J. Mech. Phys. Solids* **42** 333

[26] Mishin Y 2004 *Acta Mater.* **52** 1451

[27] Hemker K and Mills M J 1993 *Philos. Mag.* A **68** 305

[28] Schoeck G, Kohlhammer S and Fahnle M 1999 *Philos. Mag. Lett.* **79** 849

[29] Veyssiere P, Shimotomai M and Beauchamp P 1985 *Philos. Mag.* A **51** 469

[30] Paxton A and Sun Y G 1998 *Philos. Mag.* A **78** 85

[31] Karnthaler H P, Muhlbacher E T and Rentenberger C 1996 *Acta Mater.* **44** 547

[32] Sih G C and Liebowitz H in: Liebowitz H (ed) 1968 *Fracture: An Advanced Treatise* vol.2 (New York: Academic) p108

[33] Hua L, Rafii-Tabar H and Cross M 1997 *Philos. Mag. Lett.* **75** 237

[34] Machova A and Ackland G J 1998 *Modelling Simul. Mater. Sci. Eng.* **6** 521

[35] Gear C W *The Numerical Integration of Ordinary Differential Equations of Various Orders* in: 1966 Repcnt. ANL-7126. Argonne National Laboratoiy I11

[36] Fineberg J, Gross S P, Marder M and Swinney H L 1992 *Phys. Rev.* B **45** 5146

[37] Sharon E, Gross S P and Fineberg J 1995 *Phys. Rev. Lett.* **74** 5096

[38] Sharon E, Gross S P and Fineberg 1996 *J. Phys. Rev. Lett.* **76** 2117